

Generic features of a polymer quantum black hole

Johannes Münch^{1*}, Alejandro Perez^{1†}, Simone Speziale^{1‡}, Sami Viollet^{1§}

¹Aix-Marseille Université, Université de Toulon, CNRS, CPT,

13288 Marseille, France

May 26, 2023

Abstract

Non-singular black holes models can be described by modified classical equations motivated by loop quantum gravity. We investigate what happens when the sine function typically used in the modification is replaced by an arbitrary bounded function, a generalization meant to study the effect of ambiguities such as the choice of representation of the holonomy. A number of features can be determined without committing to a specific choice of functions. We find generic singularity resolution. The presence and number of horizons is determined by global features of the function regularizing the angular components of the connection, and the presence and number of bounces by global features of the function regularizing the time component. The trapping or anti-trapping nature of regions inside horizons depends on the relative location with respect to eventual bounces. We use these results to comment on some of the ambiguities of polymer black hole models.

Contents

1	Introduction	2
2	From the classical black hole to a polymerized black hole	4
2.1	Minisuperspace black hole model	4
2.2	Ashtekar-Barbero variables	9
2.3	BMM polymerisation	10
3	Generalised polymerisation	12
3.1	Presentation of the setup	12
3.2	Dirac observables	13
3.3	General expression of the metric	14

*johannes.muench@cpt.univ-mrs.fr

†alejandro.perez@cpt.univ-mrs.fr

‡simone.speziale@cpt.univ-mrs.fr

§sami.viollet@cpt.univ-mrs.fr (corresponding author)

4	Generic features of the dynamics	15
4.1	Evolution and fixed points	16
4.2	Bounces and singularity resolution	17
4.3	Horizons	19
4.4	Trapped and anti-trapped regions	20
5	Large distance behaviour	22
5.1	Asymptotic behaviour	24
5.2	Taming quantum gravity effects outside the horizon	26
6	Conclusions	27
A	Boundary term	28
B	Asymptotic expansion of the metric components	29

1 Introduction

An emblematic problem in quantum gravity is to understand the fate of the black hole singularity predicted by general relativity. Aside from extremely simplified 2d models, see e.g. [1, 2], explicit calculations are not within current reach, and this motivates the investigation of minisuperspace models in order to shed useful light on qualitative aspects of the process. In loop quantum gravity (LQG), quantum minisuperspace models are constructed using the key input from the full theory that the fundamental quantum operators are holonomies of the Ashtekar-Barbero connection. These are defined in a representation which lacks weak-continuity, thus making the models unitary inequivalent to those based on metric variables. A compelling result of this approach is the generic singularity-avoidance [3], with the minisuperspace dynamics predicting a bounce occurring at a critical energy or curvature density. This is valid in both cosmological [3, 4] and black hole [5–9] models. In the latter case, this type of investigations first started in [10, 11].

One key aspect of the construction is that the resulting quantum corrections can be equally predicted using an effective classical dynamics, where the original Hamiltonian is modified in a precise way [12]. This step is referred to as polymerization, and allows one a simple description of the system, and an independent exploration of this type of models. In spite of the compelling singularity resolutions, these models are only a first step towards a clear understanding of the non-perturbative quantum gravitational effects. To move forward, it is important to address their limitations and shortcomings. For instance, the models rely on a specific foliation, and restoring foliation-independence is far from accomplished [13–16]. The choice of polymerization scheme is not identified a priori from fundamental principles or deductions from the full theory; but rather reconstructed a posteriori requiring a good semiclassical limit at large scales, and there is no uniqueness about the procedure used [17]. We will not have much to say about the first issue, but we would like to focus on the following aspect about the second. The function used in the scheme is typically

picked to be a sine. This is supposed to represent working with the holonomy in the fundamental representation in full loop quantum gravity. However it has been known for a while that there may be quantization ambiguities associated with this choice already in the full theory [18].¹ These ambiguities affect models like [19] in which the polymerization scheme is derived from the full theory taking expectation values with respect to symmetry-reduced coherent states. The effect of such ambiguities were recently analysed in the context of quantum cosmology in [17], showing that they strongly affect the physics; here, we investigate how changes in the choice of polymer function affect static and spherically symmetric black hole models.

To that end, we focus on a specific polymer black hole model, the one proposed in [8] that we refer to as the BMM (Bodendorfer, Mele, Münch) model from here on. The model is a spherically symmetric black hole, with a four-dimensional phase space. The two configuration variables correspond to a time and an angular component of the metric. The model has the limitations mentioned above: It is based on a fixed foliation, and uses a specific choice of variables to be parametrized, identified because they realise a so-called $\bar{\mu}$ -scheme on the Ashtekar-Barbero variables. We will not touch these choices. We will instead investigate what happens if the sine functions used in the polymerization [8] are replaced by *arbitrary* functions. We expect that our techniques and the implications of our results can be applied to models of polymer quantum black holes such as [7, 8, 22–41] other than BMM.

At first sight, it may seem better to just consider explicit alternatives, e.g. changing and/or superimposing frequencies and phase shifts, in order to mimic the use of different irreducible representations of the holonomies and of different regularizing paths. But it turns out that many properties of the polymer black holes are accessible without making an explicit choice for these functions. This remarkable fact is due to the simplicity of the model, in particular the fact that one of the two Dirac observables remains simple even after polymerization. The second does not, and it makes some of our formulas implicit, without however hindering our considerations.

The two polymer functions that we keep arbitrary correspond to respectively the time and angular component of the connection. We show first of all that the configuration variables of [8] produce a $\bar{\mu}$ -scheme for any choice of polymer functions. Requiring the correct semiclassical limit at spatial infinity imposes a condition on the first derivatives of both polymer functions, but also a condition on the second derivative of the angular polymer function. Regularity of both functions avoids singularities, and replaces them with bounces. The number of bounces turns out to be determined by the angular function alone; whereas the number of horizons is determined by the time function alone. Their relative location depends on both the chosen functions and the solution considered. We provide a general graphical analysis to deduce these properties without committing to specific choices, but our analysis and formulas can be of help also in studying a specific model that one may be interested in.

Our results shows that there is a valuable richness in the class of polymer black holes, and that considerable mathematical control can be kept also relaxing the standard choice of sine polymer functions. We hope that some of this control can be used to address some of the limitations and

¹It has been recently pointed out in [20] that some of the ambiguities can be reduced by a new quantization of the Hamiltonian constraint of the full theory; nonetheless, ambiguities of the type analysed here remain in the part of the Hamiltonian constraint responsible for non-trivial propagation [21].

help constructing more robust models.

We use units $G = c = 1$.

2 From the classical black hole to a polymerized black hole

We will review the classical Schwarzschild solution, based on the Hamiltonian formulation, in order to introduce the notations commonly used in the literature. More precisely, after giving the general expression of the line element compatible with the symmetry considered (i.e. spherical symmetry and staticity) in term of the geometrodynamical variables. Then we will recall how the problem can be reformulated in terms of Ashtekar-Barbero variables and how this reformulation can lead to a new convenient set of variables, the (v, P) variables. From there, we will quickly recall the general ideas of the BMM polymerisation model which will be useful in the next part. We will highlight the main result of this model like the resolution of the singularity but we will also insist on the limitation of this model caused by the particular choices on which it is built.

2.1 Minisuperspace black hole model

We consider the following spherically symmetric and static ansatz

$$ds^2 = -\bar{a}(r)dt^2 + \frac{\bar{n}(r)}{\bar{a}(r)}dr^2 + \bar{b}^2(r)d\Omega^2. \quad (2.1)$$

The spatial diffeo constraint vanishes identically, and we eliminated the shift vector via our choice for the coordinates t, θ and ϕ . On the other hand, we have not fixed the r coordinate to be the area radius, and there is still a non-trivial Hamiltonian constraint to be solved associated with this reparametrization. Plugging this ansatz into the Einstein's equations, one finds

$$\bar{n}(r) = c_1^2 \dot{b}(r)^2, \quad \bar{a}(r) = c_1^2 \left(1 - \frac{c_2}{b(r)}\right). \quad (2.2)$$

The solution space is thus parametrized by two constants of integration, and $\bar{n}(r)$ is arbitrary. However only one of the constants has a geometrical interpretation, since c_1 can always be reabsorbed by rescaling the coordinate t . The metric in this form can be recognized to be the Schwarzschild solution, with

$$M = \frac{c_2}{2}, \quad (2.3)$$

asymptotic unit proper time $\tau := c_1 t$ and area radius b . We can freely choose a constant $\bar{n}(r) \equiv c_1^2$, and this will make r the area radius. In other words, one constant of integration is the black hole's mass, another is a rescaling of the asymptotic time, and \bar{n} is the freedom of r -reparametrizations.

The symmetry reduction makes the Einstein-Hilbert action, as well as the ensuing Poisson structure, divergent on a open topology. In the following, we will study the canonical structure of the foliation by hypersurfaces of constant r . This is because r is a time-like coordinate inside the horizon, and we are ultimately interested in the dynamics near the singularity. To regularize the action, one introduces a fiducial cell for the coordinates $x := (t, \theta, \phi)$ given by $C := [0, \ell_0] \times S^2$. The

physical size L_0 of the fiducial cell is r -dependent. Taking for instance spatial infinity as reference, we have

$$L_0 := \int_0^{\ell_0} \sqrt{|g_{tt}(r = \infty)|} dt = \ell_0 |c_1| \quad (2.4)$$

on-shell. Then,

$$S[C] = \frac{1}{16\pi} \int dr \int_C d^3x \sqrt{-g} R + \text{boundary term} = \int dr L, \quad (2.5)$$

where

$$L := \frac{\ell_0 \sqrt{\bar{n}}}{2} \left(\frac{\dot{\bar{a}} \dot{\bar{b}}}{\bar{n}} + \frac{\bar{a} \dot{\bar{b}}^2}{\bar{n}} + 1 \right). \quad (2.6)$$

The boundary term to be added to the action is the Gibbons-Hawking-York term, which takes care of eliminating derivatives on lapse and shift. For the interested reader, details are reported in Appendix A. It is convenient to reabsorb the coordinate length ℓ_0 changing variables to:

$$\sqrt{a} := \ell_0 \sqrt{\bar{a}}, \quad b := \bar{b}, \quad \sqrt{n} := \ell_0 \sqrt{\bar{n}}, \quad (2.7)$$

Notice that \sqrt{a} is the physical length of the fiducial cell in the t direction as a function of r . We end up with the following Lagrangian,

$$L(a, b, n) = \frac{\sqrt{n}}{2} \left(\frac{\dot{a} \dot{b}}{n} + \frac{a \dot{b}^2}{n} + 1 \right) \quad (2.8)$$

which will give a well-defined phase space.

At this point the spherical black hole minisuperspace model is effectively being described by a point-particle mechanical system.²

The solution space is the same as before, in particular

$$a = \ell_0^2 c_1^2 \left(1 - \frac{c_2}{b} \right). \quad (2.9)$$

However, there is an important difference about the physical interpretation of the solutions: in the point-particle description we have no longer access to the coordinate t , hence it is not possible to reabsorb c_1 with a time diffeomorphism. In other words, fiducial cells of different physical size (2.4) correspond to physically distinct points in the solution space.

Turning c_1 from an irrelevant constant to a physical one is clearly an artefact of the regularization, but it is also natural in the following sense. In the full space space, the Schwarzschild solution is a one-parameter trajectory. The smallest phase space in which this family can be embedded is 2-dimensional, hence we expect a second variable to be present and to be conjugated to the mass, and c_1 plays this role. The role of the regularization in defining this two-dimensional phase space can

²And it is part of a class of minisuperspace models described by the motion of point particles in a given supermetric, which in this case reads

$$G = \frac{2\sqrt{n}}{b} \begin{pmatrix} -a/b & 1 \\ 1 & 0 \end{pmatrix}.$$

See e.g. [42] for a description in these terms of generic spherical black holes and Bianchi models.

also be nicely understood looking at the symplectic potential obtained from the on-shell variation of (2.5), which in the area-radius gauge gives

$$\theta = -\frac{1}{2}\ell_0 (c_1 dc_2 + 2c_2 dc_1 - 2r dc_1), \quad (2.10)$$

with symplectic structure

$$\omega = \frac{\ell_0}{2} dc_1 \wedge dc_2. \quad (2.11)$$

Removing the regulator taking $\ell_0 \rightarrow \infty$ gives a divergent symplectic structure. One can also see that the commutation relation $\{c_1, c_2\} = 2/\ell_0$ has a vanishing limit, and interpret this as a sign that one of the coordinates loses its dynamical role, c_1 in this case, and can be reabsorbed into the redefinition of asymptotic time.³

We now review the Hamiltonian of the system associated with the foliation by $r = \text{constant}$ hypersurfaces. The signature of this foliation is not fixed, being time-like outside the horizon, null at the horizon, and space-like inside. No issues arise from this fact, thanks to the symmetry reduction the dynamics is well-defined for all values of r . The lapse function in the interior is

$$N(r) = \frac{\sqrt{n(r)}}{\sqrt{-a(r)}}. \quad (2.12)$$

Inspection of the Lagrangian shows that one can freely trade between N and n as Lagrange multipliers. With this choice of time, the conjugate momenta with respect to this global time parameter are

$$p_a = \frac{\partial L}{\partial \dot{a}} = \frac{b\dot{b}}{2\sqrt{n}}, \quad p_b = \frac{\partial L}{\partial \dot{b}} = \frac{2a\dot{b} + \dot{a}b}{2\sqrt{n}}, \quad p_n = \frac{\partial L}{\partial \dot{n}} = 0. \quad (2.13)$$

The last equation gives a primary constraint, that should be added to the Legendre transform of the Lagrangian. Upon doing so, one finds the primary Hamiltonian

$$H(n) = \sqrt{n} \left(\frac{2p_a p_b}{b} - \frac{2ap_a^2}{b^2} - \frac{1}{2} \right) + \lambda p_n, \quad (2.14)$$

where λ is a Lagrange multiplier. Stabilizing the primary constraint, i.e. imposing $\dot{p}_n \approx 0$, leads to the secondary constraint

$$\psi := \frac{2p_a p_b}{b} - \frac{2ap_a^2}{b^2} - \frac{1}{2} \approx 0. \quad (2.15)$$

This is the Hamiltonian constraint generating r -diffeomorphisms. It is automatically stable, and no further constraints arise in the analysis. We thus obtain a 2-dimensional physical phase space, in agreement with the two-parameter family of solutions (2.2). Moreover $\dot{n} = \lambda$, hence we can treat \sqrt{n} as a Lagrange multiplier, remove the pair (n, p_n) from the phase space and set $\lambda = 0$ without any loss of generality. Then we have a 4d kinematical phase space with Hamiltonian constraint $H(n) = \sqrt{n}\psi$. We will use this formulation from now on.

³This is the same observation already made at the quantum level in [43].

Consider now the following canonical transformation [8],

$$v_1 := \frac{2}{3}b^3, \quad P_1 := \frac{p_b}{2b^2} - \frac{ap_a}{b^3} = \frac{\dot{a}}{4\sqrt{nb}}, \quad (2.16a)$$

$$v_2 := 2ab^2, \quad P_2 := \frac{p_a}{2b^2} = \frac{\dot{b}}{4\sqrt{nb}}, \quad (2.16b)$$

$$\{v_i, P_j\} = \delta_{ij}. \quad (2.16c)$$

It is the generalization to the black hole model of a similar transformation used in loop quantum cosmology, and it will be relevant to construct the effective quantum model below. In terms of the new variables the Hamiltonian constraints becomes

$$H(n) = \sqrt{n} \left(12v_1P_1P_2 + 4v_2P_2^2 - \frac{1}{2} \right), \quad (2.17)$$

and generates the dynamical equations

$$\dot{v}_1 = 12\sqrt{n}v_1P_2, \quad (2.18a)$$

$$\dot{v}_2 = 12\sqrt{n}v_1P_1 + 8\sqrt{n}v_2P_2, \quad (2.18b)$$

$$\dot{P}_1 = -12\sqrt{n}P_1P_2, \quad (2.18c)$$

$$\dot{P}_2 = -4\sqrt{n}P_2^2. \quad (2.18d)$$

Notice that the equations for P_i are decoupled. It is also possible to easily identify two constants of motion. The first can be deduced by inspection of the Hamiltonian, and it is given by

$$K_1 = v_1P_1. \quad (2.19)$$

The second can be found taking the ratio of (2.18c) and (2.18d) and integrating, giving

$$K_2 = \ln |P_1| - 3 \ln |P_2|. \quad (2.20)$$

In performing the integration we fix the integration constants so that the two contributions to K_2 vanish when $P_1 = 1$ and $P_2 = 1$. The two constants of motion turn out to be canonically conjugated functions, $\{K_1, K_2\} = 1$, and commute with the Hamiltonian constraint by construction. Therefore they provide two Dirac observables for the system.

It is instructive to derive the Schwarzschild solution from this formulation of the dynamics, because it will help comparison with the polymerized model below. To solve the equations, let us fix its gauge freedom imposing $n = n_o$ constant, Then, (2.18d) is solved by

$$P_2(r) = \frac{1}{4\sqrt{n_o r}}, \quad (2.21)$$

up to a constant of integration that can always be absorbed by a shift of the r coordinate. This solution is valid provided $r \neq 0$. We restrict the domain to $r > 0$, hence $b > 0$. Then, using (2.20) directly leads to

$$P_1(r) = \text{sign}(P_1) \frac{e^{K_2}}{(4\sqrt{n_o r})^3}. \quad (2.22)$$

From this, (2.19), and the fact that $v_1 = \frac{2}{3}b^3 > 0$, we derive that

$$P_1(r) = \frac{\text{sign}(K_1)e^{K_2}}{(4\sqrt{n_0}r)^3} \quad \text{and} \quad v_1(r) = (4\sqrt{n_0})^3|K_1|e^{-K_2}r^3, \quad (2.23)$$

Finally, from the vanishing of the Hamiltonian constraint (2.17) we derive that

$$v_2(r) = 4\sqrt{n_0} \left(\frac{1}{2}\sqrt{n_0} - \frac{3K_1}{r} \right) r^2. \quad (2.24)$$

This general solution is of course equivalent to (2.2) found earlier. To see this explicitly, we can reconstruct the metric. Let us do so in terms of the unbarred quantities (2.7), in terms of which it reads

$$ds^2 = -\frac{a(r)}{\ell_0^2} dt^2 + \frac{n(r)}{a(r)} dr^2 + b(r)^2 d\Omega^2. \quad (2.25)$$

Inverting (2.16), we obtain

$$a = \frac{e^{2K_2/3}}{16} \left(\frac{2}{3|K_1|} \right)^{2/3} \left(1 - \frac{24 \left(\frac{3}{2}\right)^{1/3} K_1|K_1|^{1/3} e^{-K_2/3}}{b} \right), \quad (2.26)$$

$$b = 4\sqrt{n_0} \left(\frac{3|K_1|}{2} \right)^{1/3} e^{-K_2/3} r. \quad (2.27)$$

where

$$M = 2^{5/3} 3^{4/3} K_1 |K_1|^{1/3} e^{-K_2/3}. \quad (2.28)$$

We see that the metric describes the Schwarzschild solution with mass M , area radius b , and asymptotic time

$$t_S := \frac{e^{K_2/3}}{4\ell_0} \left(\frac{2}{3|K_1|} \right)^{1/3} t. \quad (2.29)$$

The solution space is spanned by all values $K_i \in \mathbb{R}^2$. Each point in this space describes a Schwarzschild black hole (with given mass—positive or negative— asymptotic time and area radius), except the line $K_1 = 0$ which describes a degenerate spacetime. The zero-mass limit corresponds to the limit $K_i \rightarrow (0^\pm, -\infty)$.

The last equation (2.27) shows that if one wants to fix the gauge $b = r$, then the constant n_0 has to be chosen in a phase-space dependent manner (note that we had already stumbled upon this fact below equation (2.3))⁴. For convenience, we also report the relation between the K_i 's and the c_i 's,

$$K_1 = \frac{\ell_0 c_1 c_2}{6} \quad K_2 = \log |16\ell_0^4 c_1^4 c_2| = \log |16\ell_0^4 c_1 c_2| + 3 \log |c_1|. \quad (2.30)$$

⁴There is a subtlety about n_0 , not relevant for the following, but useful to make contact with a discussion made in [8]. Under a change of fiducial cell $\ell_0 \mapsto \alpha\ell_0$, the function n rescales as $n \mapsto \alpha^2 n$. Under a time diffeomorphism $t \mapsto t'(t)$, it is invariant—this follows from its definition

$$\sqrt{n} := \ell_0 \sqrt{\bar{n}} = \int_0^{\ell_0} \sqrt{-g_{tt} g_{rr}} dt$$

which makes it akin to a volume quantity. Therefore, also the constant n_0 has to be chosen in an ℓ_0 -dependent way in order to preserve this properties.

From these relations we recover the results of the previous section, in particular the expression (2.3) for the mass, and c_1 being the only parameter that enters the rescaling of the asymptotic time.

Let us add a few remarks useful in the following.

- On the interpretation of the P_i variables. Using the on-shell values (2.21) and (2.23) and the relation between b and r (2.27), one finds [8]

$$P_1(b) = \frac{M}{b^3} \left(\frac{2}{3|K_1|} \right)^{1/3} \frac{e^{K_2/3}}{8}, \quad P_2(b) = \frac{1}{b} \left(\frac{3|K_1|}{2} \right)^{1/3} e^{-K_2/3}. \quad (2.31)$$

Thus P_1 is proportional to the (square root of the) Kretschmann scalar, and P_2 to the inverse area radius of the Schwarzschild black hole.

- Any phase space function that is monotonic in r will be a good clock for our Hamiltonian evolution. From the general solution, we see that all variables except v_2 are monotonic functions of r . Therefore, all of them provide good internal clocks. If we choose P_2 in particular, we can rewrite the metric in a lapse-independent way,

$$ds^2 = -\frac{1}{16} \left(\frac{2e^{K_2}}{3K_1} \right)^{2/3} (1 - 24K_1P_2) d\tau^2 + \left(\frac{3K_1\lambda_1}{2\lambda_1P_1} \right)^{2/3} (1 - 24K_1P_2)^{-1} \lambda_2^2 dP_2^2 + \left(\frac{3K_1\lambda_1}{2\lambda_1P_1} \right)^{2/3} d\Omega^2, \quad (2.32)$$

$$\tau := \frac{t}{\ell_0} \quad (2.33)$$

This is the form of the metric that we will write below for the polymerized model.

2.2 Ashtekar-Barbero variables

The first step towards polymerisation is a canonical transformation to Ashtekar-Barbero variables,

$$A_a^i := \Gamma_a^i + \gamma K_a^i, \quad E_i^a = \frac{1}{2} \epsilon_{ijk} \epsilon^{abc} e_b^j e_c^k, \quad (2.34)$$

where γ is the Immirzi parameter. For the interior of a spherically symmetric and static spacetime we can take them to be [7, 27, 32]⁵

$$A_a^i \tau_i dx^a = \frac{c(r)}{\ell_0} \tau_3 dt + d(r) \tau_2 d\theta - d(r) \tau_1 \sin \theta d\phi + \tau_3 \cos \theta d\phi, \quad (2.35)$$

$$E_i^a \tau^i \partial_a = p_c(r) \tau_3 \sin \theta \partial_t + \frac{p_d(r)}{\ell_0} \tau_2 \sin \theta \partial_\theta - \frac{p_d(r)}{\ell_0} \tau_1 \partial_\phi, \quad (2.36)$$

⁵With the renaming $b(r) \mapsto d(r)$ to avoid confusion with our $b(r)$ defined in (2.1) and (2.7).

where $\tau_i = (-i/2)\sigma_i$ and σ_i are the Pauli matrices. The map to the previous variables is given by

$$\text{sign}(p_c) c = -2\gamma \left(\frac{p_b}{2b} - \frac{ap_a}{b^2} \right) = -2\gamma P_1 \left(\frac{3v_1}{2} \right)^{1/3}, \quad (2.37a)$$

$$\text{sign}(p_d) d = 2\gamma \frac{\sqrt{-ap_a}}{b} = 4\gamma P_2 \sqrt{-\frac{v_2}{2}}, \quad (2.37b)$$

$$\text{sign}(p_c) p_c = b^2 = \left(\frac{3v_1}{2} \right)^{2/3}, \quad (2.37c)$$

$$\text{sign}(p_d) p_d = \sqrt{-ab} = \sqrt{-\frac{v_2}{2}}. \quad (2.37d)$$

The overall sign ambiguity is the usual global parity freedom in the triad, whereas the relative sign ambiguity is a consequence of the symmetry reduction, and cannot be eliminated [?]. This map is a canonical transformation, with non vanishing Poisson brackets given by

$$\{c, p_c\} = 2\gamma, \quad \{d, p_d\} = \gamma, \quad (2.38a)$$

and Hamiltonian constraint

$$H(N) = -\frac{Nd}{2\gamma^2 \text{sign}(p_c) \sqrt{|p_c|}} \left(2cp_c + \left(d + \frac{\gamma^2}{d} \right) p_d \right). \quad (2.39)$$

As before lapse is related to our choice of Lagrange multiplier n by (2.12), a redefinition which does not affect the equations of motion.⁶

2.3 BMM polymerisation

The BMM model [8] is based on the (v_i, P_i) phase space variables we reviewed above. There are two key observations made in [8] that motivate the use of these variables. The first is that as we observed above, P_1 is related to the Kretschmann scalar and P_2 to the inverse area radius. Hence we could intuitively expect that replacing these variables by bounded functions should remove the classical divergences of the dynamics. The second is that polymerizing these variables with a non-dynamical regulator induces a $\bar{\mu}$ -scheme on the Ashtekar-Barbero variables, compatible with the Hamiltonian. Hence these variables are the analogue of the (v, b) variables in loop quantum cosmology. To see this, consider the replacement

$$P_i \rightarrow \frac{\sin(\lambda_i P_i)}{\lambda_i}, \quad i = 1, 2, \quad (2.40)$$

where λ_1 and λ_2 are a priori independent polymerisation scales (i.e. the scale at which the modification of the dynamic will be important). We take them to be constants, and of Planckian order. From (2.37) we have that

$$\lambda_1 P_1 = \delta_c c, \quad \delta_c := -\text{sign}(p_c) \frac{\lambda_1}{2\gamma \sqrt{|p_c|}}, \quad (2.41)$$

$$\lambda_2 P_2 = \delta_d d, \quad \delta_d := \text{sign}(p_d) \frac{\lambda_2}{4\gamma |p_d|}. \quad (2.42)$$

⁶Hamilton's equations are modified by the addition of a term proportional to the constraint and thus zero on-shell.

Hence the replacement (2.40) is equivalent to

$$c \rightarrow \frac{\sin(\delta_c c)}{\delta_c}, \quad d \rightarrow \frac{\sin(\delta_d d)}{\delta_d d}, \quad (2.43)$$

where the quantum parameters δ_c and δ_d have a phase-space dependance given by (2.41). This phase-space dependance can be used to introduce the area-gap of the full theory, thus defining a $\bar{\mu}$ -scheme for the Ashtekar-Barbero variables. The replacement (2.40) leads to the modified Hamiltonian constraint

$$H_{\text{eff}}(n) = \sqrt{n} \mathcal{H}_{\text{eff}} \quad , \quad \mathcal{H}_{\text{eff}} = 12v_1 \frac{\sin(\lambda_1 P_1)}{\lambda_1} \frac{\sin(\lambda_2 P_2)}{\lambda_2} + 4v_2 \frac{\sin(\lambda_2 P_2)^2}{\lambda_2^2} - \frac{1}{2} \approx 0. \quad (2.44)$$

On the other hand, the polymerization of the Ashtekar-Barbero Hamiltonian (2.39) under (2.43) gives

$$H_{\text{eff}}(N) = -\frac{N \sin(\delta_d d)}{\delta_d 2\gamma^2 \text{sign}(p_c) \sqrt{|p_c|}} \left(2 \frac{\sin(\delta_c c)}{\delta_c} p_c + \left(\frac{\sin(\delta_d d)}{\delta_d} + \frac{\gamma^2 \delta_d}{\sin(\delta_d d)} \right) p_d \right).$$

Inserting (2.41), (2.37) and (2.12) in the latter recovers the former, therefore the polymerization (2.40) is consistent with the $\bar{\mu}$ -scheme also at the dynamical level.

The dynamics generated by the polymerized Hamiltonian is expected to capture the mean field quantum corrections [12] and it is thus referred to as effective dynamics. This effective dynamics is obtained from (2.44) and the original Poisson brackets (2.16c), giving

$$\dot{v}_1 = 12\sqrt{n}v_1 \cos(\lambda_1 P_1) \frac{\sin(\lambda_2 P_2)}{\lambda_2}, \quad (2.45a)$$

$$\dot{v}_2 = 12\sqrt{n}v_1 \frac{\sin(\lambda_1 P_1)}{\lambda_1} \cos(\lambda_2 P_2) + 8\sqrt{n}v_2 \frac{\sin(\lambda_2 P_2)}{\lambda_2} \cos(\lambda_2 P_2), \quad (2.45b)$$

$$\dot{P}_1 = -12\sqrt{n} \frac{\sin(\lambda_1 P_1)}{\lambda_1} \frac{\sin(\lambda_2 P_2)}{\lambda_2}, \quad (2.45c)$$

$$\dot{P}_2 = -4\sqrt{n} \frac{\sin(\lambda_2 P_2)^2}{\lambda_2^2}, \quad (2.45d)$$

$$\mathcal{H}_{\text{eff}} = 3v_1 \frac{\sin(\lambda_1 P_1)}{\lambda_1} \frac{\sin(\lambda_2 P_2)}{\lambda_2} + v_2 \frac{\sin(\lambda_2 P_2)^2}{\lambda_2^2} - \frac{1}{8} = 0. \quad (2.45e)$$

It was shown in [8] that the equations can be solved analytically, and the following properties ensue:

1. The singularity at $b = 0$ is removed.
2. There are two asymptotic spacetime regions, both approaching a Schwarzschild geometry.
3. There is a space-like surface at some $b_{\text{min}} \neq 0$ inside the horizon, which is the a global minimum of the area radius b and corresponds to a black-to-white hole transition.
4. There are two independent Dirac observables, which can be physically interpreted as the masses of the separate asymptotic Schwarzschild regions, namely of the black and of the white hole masses respectively.
5. The horizon is slightly smaller than the classical result (for black hole masses large w.r.t. the polymerisation scales).

6. For black hole masses comparable or smaller of the polymerisation scales, there are large quantum effects at the horizon scale.
7. There is an upper bound to the curvature, as measured for instance by the Kretschmann scalar, and this value is obtained at the transition surface and depends on the black holes mass (as well as the white hole mass), unlike in the prior polymerization scheme of [7] or in other models of non-singular black hole [44]

This model has the nice feature that shows how an LQG–inspired quantization can lead to a resolution of the singularity and its explicit replacement by a (non-necessarily symmetric) black-hole-to-white-hole transition, a scenario suggested in [45]. A possible shortcoming of the model is that the scale at which quantum effects become large depends on the parameters, and a certain restriction on the masses is necessary if one wants to confine this scale to inside the horizon.⁷ On the other hand, the model is based on several arbitrary choices:

- (i) A specific foliation of the spacetime has been fixed, given by the level sets of the r coordinate in Schwarzschild coordinates, and it has been shown that different foliations can give different physical results [46].
- (ii) A specific $\bar{\mu}$ -scheme, based on the polymerisation of the two P_i variables, neither more nor less.
- (iii) The polymerisation function for both variables is a sine function, in analogy with LQC models.

These choices are common, and indeed motivated by, the literature (see e.g. [7, 23–25, 27]). However, more general recent proposals exist, see e.g. [32]. Testing the robustness of the results with different choices, and conversely identifying choices that reduce the shortcomings, is crucial to move forward in the study of such models. In the rest of this paper we focus on (iii), and study the effect of changing the polymerisation function.

3 Generalised polymerisation

3.1 Presentation of the setup

To preserve the LQG-inspired idea of a polymer quantisation, it is sufficient to restrict the polymerisation function to a generic function (for a general discussion of this ambiguity see [18], for its study in quantum cosmology see [17]). Consequently, we consider a generic replacement

$$P_i \rightarrow \frac{f_i(\lambda_i P_i)}{\lambda_i}, \quad (3.1)$$

where f_1 and f_2 are real, bounded, C^1 and periodic functions of periodicity 2π , and such that $f_i(x) = x + o(x)$, that is

$$f_i(0) = 0, \quad (3.2a)$$

$$f'_i(0) = 1, \quad (3.2b)$$

⁷This situation arises in other proposals as well [29]. An attempt to improve this situation has been made in [29, 30].

with the notation $f'_i = \frac{df_i(\lambda_i P_i)}{d(\lambda_i P_i)}$. Below in Section 5.1 we will prove that these conditions are necessary in order to recover the Schwarzschild solution in the large distance limit, but not sufficient: one further needs $f''_2(0) = 0$. This additional condition however does not affect qualitatively the short distance structure, hence we will only introduce it when needed explicitly. Following this replacement, the new polymerized Hamiltonian is given by

$$H_{\text{eff}} = \sqrt{n} \mathcal{H}_{\text{eff}}, \quad \mathcal{H}_{\text{eff}} := 12v_1 \frac{f_1(\lambda_1 P_1)}{\lambda_1} \frac{f_2(\lambda_2 P_2)}{\lambda_2} + 4v_2 \frac{f_2^2(\lambda_2 P_2)}{\lambda_2^2} - \frac{1}{2} \approx 0, \quad (3.3)$$

In the limit $\lambda_i P_i \rightarrow 0$ we recover the classical Hamiltonian, thanks to the required linear behaviour around the origin.

The polymerized dynamical equations are

$$\dot{v}_1 = 12\sqrt{n}v_1 f'_1 \frac{f_2}{\lambda_2}, \quad (3.4a)$$

$$\dot{v}_2 = 12\sqrt{n}v_1 \frac{f_1}{\lambda_1} f'_2 + 8\sqrt{n}v_2 \frac{f_2}{\lambda_2} f'_2, \quad (3.4b)$$

$$\dot{P}_1 = -12\sqrt{n} \frac{f_1}{\lambda_1} \frac{f_2}{\lambda_2}, \quad (3.4c)$$

$$\dot{P}_2 = -4\sqrt{n} \frac{f_2^2}{\lambda_2^2}, \quad (3.4d)$$

$$\mathcal{H}_{\text{eff}} = 3v_1 \frac{f_1}{\lambda_1} \frac{f_2}{\lambda_2} + v_2 \frac{f_2^2}{\lambda_2^2} - \frac{1}{8} \approx 0. \quad (3.4e)$$

They generalize (2.45) in a straightforward way. Remarkably, it is possible to solve these equations in full generality without specifying the functions f_i , even though in a partially implicit way. The knowledge of the implicit general solution will be sufficient to describe a large number of features of the modified spacetime generated by f_1 and f_2 . The first step to construct this solution is to identify the Dirac observables.

3.2 Dirac observables

Dirac observables are gauge independent quantities, namely they Poisson-commute with all the constraints. The only constraint of our model is \mathcal{H}_{eff} (cfr. Eq. (3.3)), which also generates the dynamics. Dirac observables will coincide with constants of motion, thus their identification leads immediately to the general solution of the equations of motions. More precisely, the expressions for the Dirac observables plus the constraints provide sufficient implicit relations to determine all phase space variables in terms of a chosen internal clock.

As the kinematical phase space is four-dimensional and we have one first class constraint, there are at most two independent Dirac observables. These were referred to as K_i in the non-polymerized case, and we keep the same notation. They can be identified proceeding as in the non-polymerized case. The first can be found by inspection of the Hamiltonian constraint (3.3) to be

$$K_1 := v_1 \frac{f_1}{\lambda_1}. \quad (3.5)$$

Recall further, that v_1 is closely related to the area radius b (cfr. Eq. (2.16)). Therefore, this Dirac observable will be useful to analyse the area radius as a function of P_1 and to make statements

about possible bounces and black-to-white hole transitions (see Sec. 4.2 below). For the second Dirac observable again we divide (3.4c) by (3.4d) and integrate, obtaining as before

$$K_2(P_1, P_2) = \lambda_1 \int_1^{P_1} \frac{dP_1}{f_1(\lambda_1 P_1)} - 3\lambda_2 \int_1^{P_2} \frac{dP_2}{f_2(\lambda_2 P_2)}. \quad (3.6)$$

This constant of motion is well-defined for any choice of polymer function. However its explicit form can only be accessed once the functions are specified. The choice of lower bound in the integrals is made once and for all and it is needed to fix the freedom of constant shifts of Dirac observables. Here we picked 1 in agreement with the choice made in (2.20).

3.3 General expression of the metric

To solve the dynamics in terms of the Dirac observables, we will start by noticing that the Hamiltonian constraint (3.3) imposes that f_2 can never vanish on solutions. Consequently, the equation (3.4d) implies that P_2 is a strictly decreasing function of r . It is thus a good internal clock, and we use it to deparametrise the equations of motion,⁸ and rewrite the metric coefficients as $a(P_2)$ and $b(P_2)$. Notice that with this choice the metric will be independent of the lapse, see (2.32). The coordinate r and P_2 are related via (3.4d)

$$dr = -\frac{\lambda_2^2}{4\sqrt{n}f_2^2} dP_2. \quad (3.7)$$

Next, we want to determine the metric coefficients in (2.25) as functions of P_2 . To that end, b can be expressed in terms of P_1 using the first Dirac observable (3.5) and (2.16a), leading to

$$b(P_1) = \left(\frac{3\lambda_1 K_1}{2f_1} \right)^{1/3}. \quad (3.8)$$

This can be turned into a function of P_2 using the implicit relation $P_1 = P_1(\lambda_2 P_2, K_2)$ determined by picking a specific value K_2 for the second Dirac observable (3.6). To make this step clear, we will use the following notation,

$$f_1(\lambda_1 P_1(\lambda_2 P_2, K_2)) = g_1(\lambda_2 P_2, K_2). \quad (3.9)$$

To determine a , we use the Hamiltonian constraint (3.3) to write

$$v_2 = \frac{\lambda_2^2}{8f_2^2} - \frac{3K_1\lambda_2}{f_2}. \quad (3.10)$$

Plugging this expression in (2.16) we find

$$a = \left(\frac{2f_1}{3\lambda_1 K_1} \right)^{2/3} \left(\frac{\lambda_2^2}{16f_2^2} - \frac{3K_1\lambda_2}{2f_2} \right). \quad (3.11)$$

⁸Note that this is possible at the effective level as here we have access to P_2 directly. At the polymer quantum level P_2 is not available and this de-parametrisation would have to be reconsidered.

This way all metric components are expressed in terms of the Dirac observables K_i and the internal clock P_2 , and the metric (2.25) reads⁹

$$ds^2 = - \left(\frac{2g_1}{3K_1\lambda_1} \right)^{2/3} \left(\frac{\lambda_2}{4f_2} \right)^2 \left(1 - \frac{24K_1f_2}{\lambda_2} \right) d\tau^2 + \left(\frac{3K_1\lambda_1}{2g_1} \right)^{2/3} \left(1 - \frac{24K_1f_2}{\lambda_2} \right)^{-1} \lambda_2^2 dP_2^2 + \left(\frac{3K_1\lambda_1}{2g_1} \right)^{2/3} d\Omega^2, \quad (3.12)$$

with $\tau = t/\ell_0$ as before.

Note that the Dirac observable K_1 appears explicitly in this line element, while K_2 enters only implicitly via the definition of g_1 , see Eq. (3.9). Once the polymer functions f_i have been specified, one can compute the integrals (3.6) and obtain $P_1(P_2)$. This will make g_1 explicit and thus the metric. It is quite remarkable that one can write the metric line element for completely arbitrary polymer functions, albeit with the limitation of an implicit function explained above. It means that one can deduce a great deal of the properties of the models without committing to specific choices too soon, and this is what we investigate next. As a sanity check, replacing the polymer functions by their arguments recovers the metric (2.32), namely the Schwarzschild solution. The polymerized metrics on the other hand are obviously not solutions of the Einstein's equations, and as we show in the next Section, describe spacetimes with a varying number of horizons and bounces, depending on the polymer functions as well as the Dirac observables. A feature that remains from the unpolymerized model is that $K_1 = 0$ describes metrics everywhere degenerate. In the following Section 5.1, we will show that even if the metrics do not describe a classical black hole, the Schwarzschild metric is recovered in the large radius limit, provided the condition $f_2''(0) = 0$ is satisfied.

In order to do so, it is convenient to express the metric using the area radius as coordinate, as opposed to P_2 . However, the polymerization makes $b(P_2)$ a non-monotonic function. This is known already for the sine functions [8], and will become clear during the analysis of (3.4) in the next Section. The area radius coordinate will have to be independently defined in different branches. On each of these branches, we have

$$ds^2 = -\frac{1}{b^2} \left(\frac{\lambda_2}{4f_2} \right)^2 \left(1 - \frac{24K_1f_2}{\lambda_2} \right) d\tau^2 + \frac{1}{f_1'^2} \left(1 - \frac{24K_1f_2}{\lambda_2} \right)^{-1} db^2 + b^2 d\Omega^2 \quad (3.13)$$

In other words, (3.12) is the maximal extension, and (3.13) the expression valid in each area radius patch.

4 Generic features of the dynamics

In this Section we study the geometry of the polymer spacetime (3.12). We show that it is possible to work out several features such horizons, bounces, and singularity resolution without specifying the polymerisation functions. We start by analysing the equations of motion as a dynamical system, in order to identify the asymptotic regions and relative locations of the spacetime features.

⁹Note that all factors of n dropped out, which was expected as this is a pure gauge freedom specifying the coordinate r , which was replaced by the intrinsic clock P_2 .

4.1 Evolution and fixed points

We proceed as follows. First, we eliminate the v_i variables using respectively K_1 and the Hamiltonian constraint. We then focus on the restricted space spanned by P_i , with equations of motion (3.4c) and (3.4d). Notice that $P_2 \neq 0$, otherwise the Hamiltonian constraint is violated as a consequence of (3.2). We also exclude $P_1 = 0$, because again from (3.2) it implies $K_1 = 0$ and as shown earlier these points describe degenerate metrics.

To study the restricted space of the dynamics of the P_i 's, it is convenient to fix the lapse to

$$\sqrt{n} = \frac{\lambda_2}{4f_2}, \quad (4.1)$$

because it decouples the equations of motion. This gauge choice is always accessible, as the Hamiltonian constraint (3.3) implies $f_2(\lambda_2 P_2) \neq 0$ throughout the evolution. The dynamical flow is then described by the simple vector field

$$V(P_1, P_2) = \begin{pmatrix} \dot{P}_1 \\ \dot{P}_2 \end{pmatrix} = \begin{pmatrix} -3f_1/\lambda_1 \\ -f_2/\lambda_2 \end{pmatrix}. \quad (4.2)$$

We have already argued that f_2 can never vanish on solutions, because otherwise the Hamiltonian constraint is violated. On the other hand f_1 can vanish, but if it does, $K_1 \equiv 0$, and the motion is then confined on points which describe only degenerate metrics. Excluding degenerate metrics, the polymer functions can never vanish along the solutions. This key property implies that there are no fixed points to the dynamical system, and that the P_i 's plane is partitioned into a check-board given by the zeros of the f_i 's, with the dynamics being trapped inside each square. See Fig. 1, left panel, for an illustration. Notice that what matters is the zeros, not the period, of the f_i 's. If there are zeros before the period, one obtains an irregular check-board with some squares smaller than others, see the right panel of the figure. Furthermore, the evolution of the P_i 's is *monotonic* between the extrema allowed. This allows us to get a pretty clear qualitative picture of the dynamics. We focus on the four squares of the check-board connected to the origin, since they are the only ones that contain the classical regime $\lambda_i P_i \ll 1$. Even though the origin in itself is not an allowed configuration, it plays the role of an asymptotic fixed point, as we now show.

Near the origin the f_i 's have a linear behaviour, hence (4.2) gives $\text{sgn}(\dot{P}_i) = \text{sgn}(P_i)$. Not only the evolution is monotonic, but it is also tied to the sign of P_i . Therefore if we trace it backwards it will tend towards the origin, whichever of the 4 squares we are on. The origin must thus be a repulsive fixed point. It is actually an asymptotic fixed point, since the point itself is excluded from the phase space. The monotonic evolution without fixed points then forces the system to reach the farthest corner (across the diagonal of the square) for each square, see again Fig. 1. These corners are thus attractive asymptotic fixed points.

The above description can be completed with an explicit perturbative expansion around the (asymptotic) fixed points. To that end, we posit

$$P_i(r) = \overset{\circ}{P}_i + \delta P_i(r), \quad (4.3)$$

where $\overset{\circ}{P}_i$ are zeros of f_i , and we Taylor-expand the polymer functions for $\lambda_i \delta P_i \ll 1$ around $\overset{\circ}{P}_i$. At

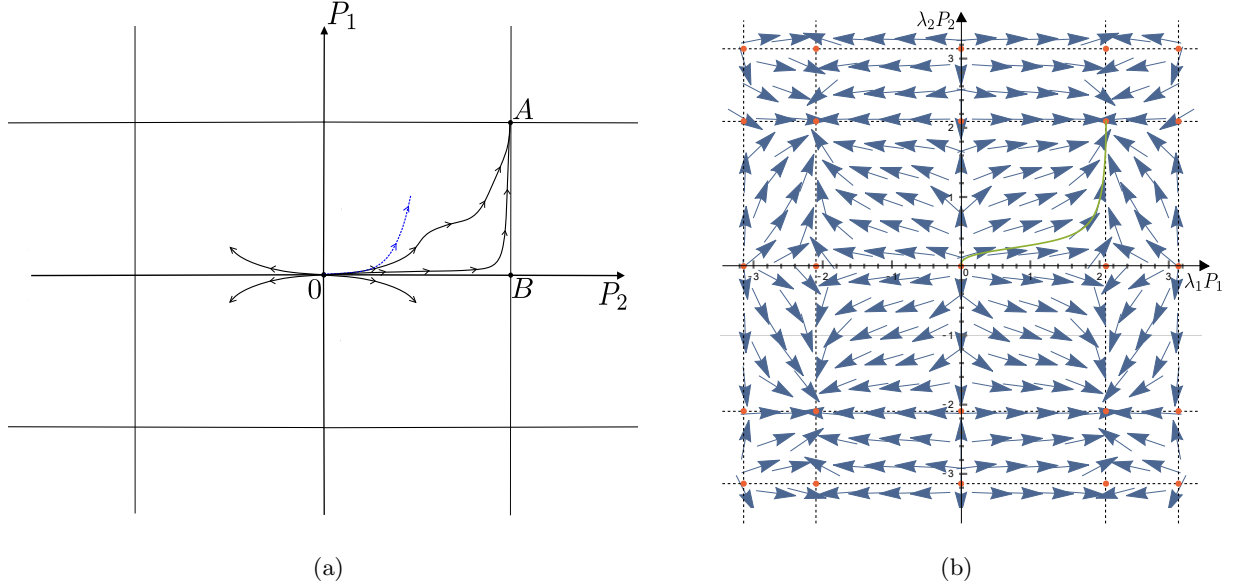


Figure 1: (a) Qualitative picture of generic dynamics. The horizontal and vertical straight lines are the zeros of f_1 and f_2 respectively. The trajectories are monotonic in both variables within each square. The vertices of the check-board are alternatively repulsive and attractive asymptotic fixed points, like the origin and the point A , or unstable points like B . For reference, the blue dashed line is the relation in the case of the classical Schwarzschild solution. (b) Flow generated by the vector field V with $f_1(x) = f_2(x) = (\sin(x) + \sin(2x))/3$. In this example, an additional zero is present inside one period of each polymer function, hence the check-board of confined evolution has squares smaller than the period, and of different sizes. The (asymptotic) fixed points are marked with red dots.

leading order, (4.2) simplifies to

$$\delta \dot{P}_1 = -3 \overset{\circ}{f}'_1 \delta P_1, \quad \delta \dot{P}_2 = -\overset{\circ}{f}'_2 \delta P_2, \quad (4.4)$$

whose solutions are

$$\delta P_1 = \delta \overset{\circ}{P}_1 e^{-3 \overset{\circ}{f}'_1 r}, \quad \delta P_2 = \delta \overset{\circ}{P}_2 e^{-\overset{\circ}{f}'_2 r}. \quad (4.5)$$

From conditions (3.2b) we conclude that the exponents are negative, meaning that the classical regime is reached for $r \rightarrow \infty$. Conversely, the farthest corner must have negative derivatives (because it is the next zero of the function), hence it is reached for $r \rightarrow -\infty$. The remaining two corners of each square are unstable fixed points with one positive and one negative derivative.

This analysis can also be used to show that the area radius is not a monotonic function of P_2 , and therefore not of r . In fact, we see from (3.8), and the periodicity of f_1 , that b is not a monotonic function of P_1 , and the monotonicity of the P_i as a function of r implies that also $P_1(P_2)$ is monotonic. Therefore, the inversion $P_2(b)$ can only be done for each of the branches, as illustrated in Fig. 2.

4.2 Bounces and singularity resolution

The notion of bounce can be visualized if we keep in mind the parallel between a black hole and a Kantowski-Sachs cosmological spacetime: a bounce is associated to a local minimum of the area

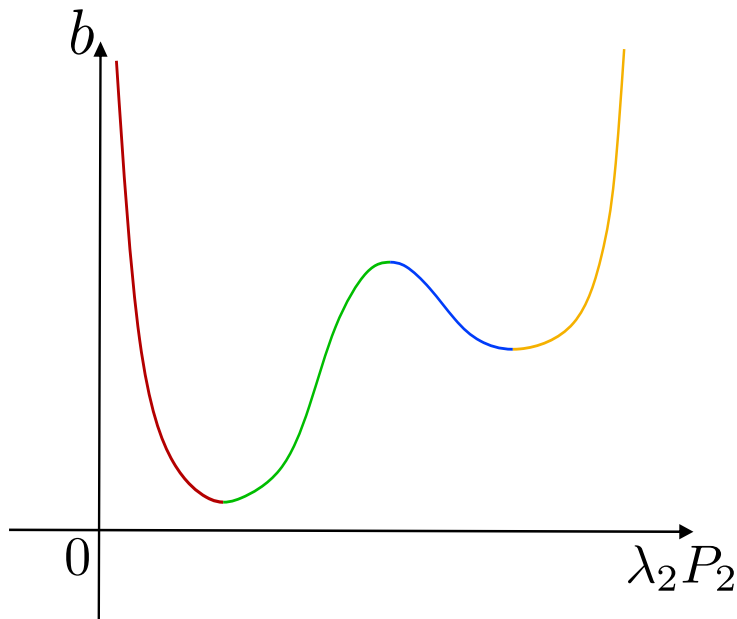


Figure 2: Plot of the area radius as a function of $\lambda_2 P_2$. Different colours are used to separate the branches where the function $b(\lambda_2 P_2)$ is invertible.

radius $b(r)$. We will see in this Section that the location and number of bounces depends only on f_1 . In the next Section we will see that the location and number of Killing horizon is determined by f_2 instead.

The evolution equation for the area radius given by (3.4a) is monotonic until we hit an extremum of f_1 , namely a point such that

$$f_1' = 0, \quad f_1'' \neq 0. \quad (4.6)$$

At this point the evolution turns around, and we have a bounce if it was initially decreasing, and a anti-bounce or turning point if it was increasing. Existence of at least one such point is guaranteed by the requirement of periodicity of f_1 . So the bounce is guaranteed, but we can have as many bounces and counter-bounces (or turning points) as we want, choosing the appropriate f_1 . Furthermore, boundness of f_1 implies that that $b = 0$ is only accessible for the solutions with vanishing K_1 and those are everywhere degenerate. Therefore the bounce must occur before reaching zero area radius. This suggests that the Schwarzschild singularity is resolved. To look into the question of singularities more precisely, one can evaluate the Kretschmann scalar associated with (3.12). This can be done explicitly with the aid of an algebraic manipulator like Mathematica or Maple. The result has the following form,

$$R_{\mu\nu\rho\sigma}^2 = \frac{F(g_1, f_2)}{f_2^4 g_1^{8/3}}, \quad (4.7)$$

where F is a six-order polynomial in g_1 , f_2 and their first and second derivatives. If we take polymerisation functions that are periodic and C^2 , the numerator in the previous expression is finite. The only divergences can arise from zeros of g_1 or f_2 . These do occur, but at points that we have identified as the asymptotes for $r \rightarrow \pm\infty$. Let us examine them separately. The first of these

is the origin in P_i space (see Fig. 1) where we know that the solution describes the Schwarzschild metric at $r \rightarrow \infty$ with finite (indeed vanishing) Kretschmann invariant. For the opposite corners, we don't have a general argument for finiteness. However these points correspond to $r \rightarrow -\infty$, therefore in so far as this limit describes the post-bounce behaviour of another asymptotically flat spacetime, it will be non-singular. We conclude that the only singularities allowed by these polymer models with smooth f_i 's are big-rip-type singularities, and require polymer functions such that the curvature diverges at $r \mapsto -\infty$.

Of course in the case where the spacetime is also a Schwarzschild spacetime around this fixed point, the Kretschmann scalar will be finite also near this fixed point. This case is particularly interesting since it corresponds to a black to white hole transition. We will see in the following how to choose the polymerization functions f_1 and f_2 to obtain this situation. This type of argument can in principle be extended to other curvature scalars and it is an indication of the absence of singularities away from asymptotic points in these models.

4.3 Horizons

The number of horizons depends on f_1 alone, and their location on both f_i . From the general form (2.25) of the metric, we know that ∂_t is a Killing vector, therefore there is a Killing horizon whenever $a = 0$. From (2.16b) and the fact that $b \neq 0$ everywhere, this condition is equivalent to $v_2 = 0$. Using then the Hamiltonian constraint (3.3), this translates to

$$f_2 = \frac{\lambda_1 \lambda_2}{24v_1 f_1} = \frac{\lambda_2}{24K_1}. \quad (4.8)$$

It is clear that it is possible to get any number of horizons, depending on the choice of f_2 and the value of K_1 . Fig. 3 shows an example of polymer function admitting four horizons. Since f_2 is

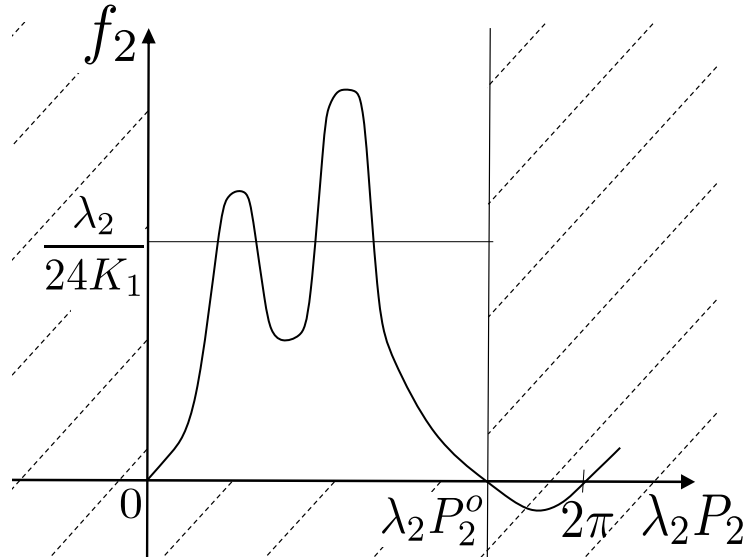


Figure 3: Sketch of an arbitrary example polymerisation function for f_2 . Only the non-shaded region between $\lambda_2 P_2 = 0$ and $\lambda_2 P_2^0$ is relevant for the dynamics. The horizons correspond to the intersection of the function f_2 and the horizontal line $\frac{\lambda_2}{24K_1}$, explicitly depends on the chosen solution and the value K_1 .

bounded, there always exist values of K_1 for which there are no horizons. The bound in order to have at least one horizon is

$$K_1 \geq \frac{\lambda_2}{24 \max f_2}. \quad (4.9)$$

It follows that while the unpolymerized solution space describes always Schwarzschild black holes, of different mass and asymptotic time, the polymerized solution space always contains (non-singular) black holes as well as spacetimes without horizons (or exotic quantum stars).

A non-singular black hole scenario well considered in the literature is the black-to-white transition [8, 27, 45, 47, 48], in which two event horizons sit on either side of a bounce. Since polymer functions realize this scenario already [8]. One can then ask the question if the realization of this scenario imposes interesting restrictions on the polymer functions, and how much the scenario can be generalized allowing arbitrary polymer functions. From the analysis just done, we see that the black-to-white transition corresponds to having a maximum of $f_1(P_1(P_2))$ between two intersections of $f_2(P_2)$ with K_2 . No further requirement is needed. Therefore the freedom/ambiguity in the polymer functions cannot significantly be constrained by requiring that such scenario be realized. Conversely, all sorts of modifications of the scenario are possible by playing with global features of the regularization functions. The simplest qualitative novelty that can be introduced changing f_i from the sine function is an asymmetry between the contracting phases. More in general, it is possible to combine multiple bounces and multiple horizons.

In all cases, the relative location of bounces and horizons is not fixed, and will depend on both the choice of polymer functions and initial conditions. If the system is explicitly solved, the relative location can straightforwardly be determined from the functions $P_i(r)$. Interestingly, it is possible to find the relative location of bounces and horizons even without knowing the explicit solutions $P_i(r)$. This follows from the fact that the trajectories must satisfy the identity

$$3 \int_{\lambda_2 P_2(r_0)}^{\lambda_2 P_2(r)} \frac{dx}{f_2(x)} = \int_{\lambda_1 P_1(r_0)}^{\lambda_1 P_1(r)} \frac{dx}{f_1(x)}, \quad (4.10)$$

as it follows from the constancy of the Dirac observable K_2 defined in (3.6). Given two reference values $P_i(r_0)$, this equation can be used to find the value of say $P_2(r)$ as a function of $P_1(r)$. To show how this is done in practise, consider the example of one bounce and two horizons, with polymer functions depicted in Fig. 4. We want to establish if the bounce occurs in between the horizons, or outside. To bring out the dependence on the initial conditions, we can choose a value for r_0 in the classical domain, so that an approximate explicit solution is known, given by (2.21) and (2.23). Equation (4.10) fixes in this way $P_2(r_b)$ as a function of $P_1(r_b)$ and classical inputs and can be used to determine the position of the bounce with respect to the horizons present in the effective geometry, as illustrated on Fig. 5. All this depends explicitly on the choice of the polymer functions and Dirac observables K_1 and K_2 . The analysis holds for multiple bounces and multiple horizons.

4.4 Trapped and anti-trapped regions

In a black-to-white hole transition, the bounce separates a trapped and anti-trapped region between the two corresponding horizons. We now show that the nature of the trapping or anti-trapping region turns out to be very simply determined by the sign of f'_1 . More general cases, for instance if both horizons are on the same side of the bounce, would require a systematic analysis.

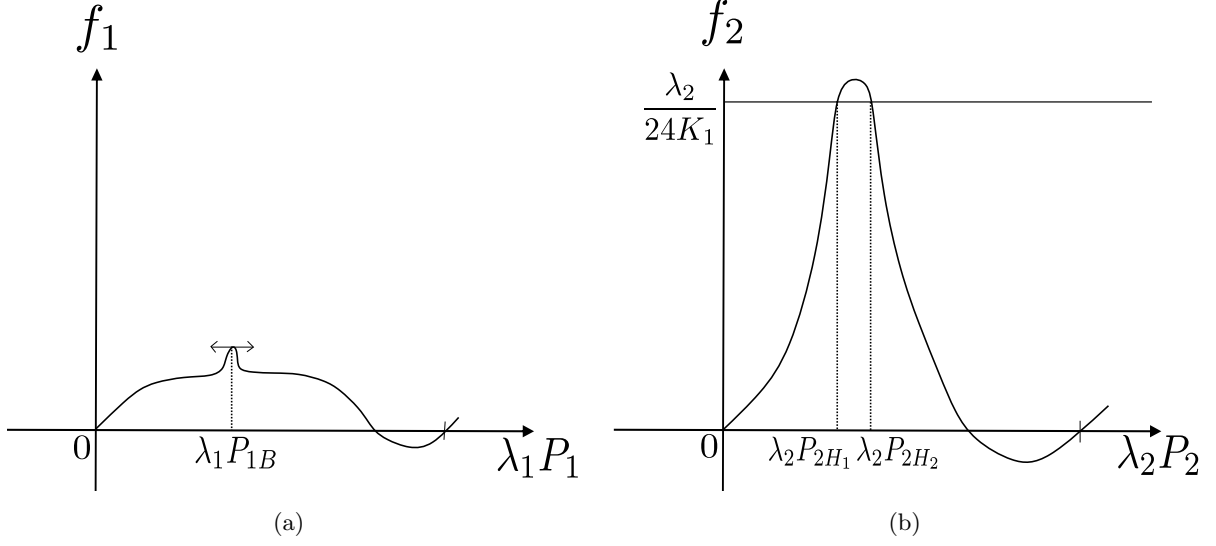


Figure 4: (a) Plot of a specific polymerisation function for f_1 with only one local maximum between its two first zeros, i.e. only one bounce can appear (b) Plot of a specific polymerisation function for f_2 with only one local maximum between its two first zeros. Depending on the choice made for the Dirac observable K_1 , at most two horizons will appear.

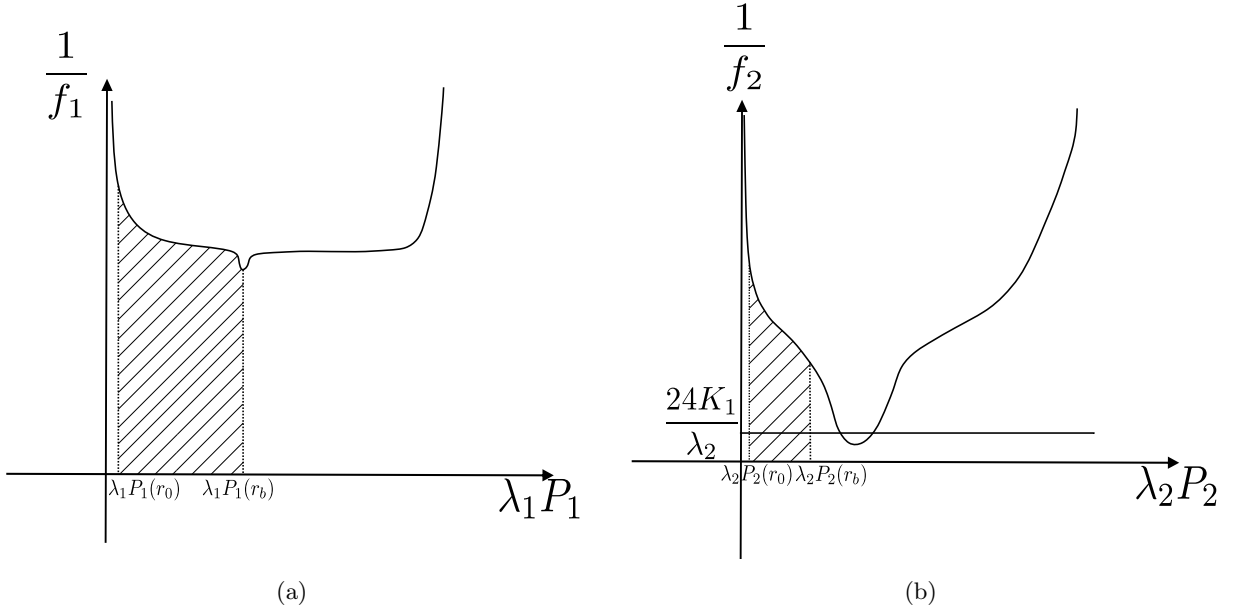


Figure 5: Plot of the inverse of the polymerisation functions where the dashed area correspond to the integrals in (4.10).

To see this, we recall that the outgoing and incoming expansions of null geodesic congruences

	$\text{sign}(\dot{b}) = -$	$\text{sign}(\dot{b}) = +$
$\text{sign}(a) = -$	Anti-trapped	Trapped
$\text{sign}(a) = +$	Free	Free

Table 1: Summary of the causal structure of a region in term of the sign of a and b . These results come from (4.11) and (4.12)

for the spherical metric (2.1) are given by (see e.g. [8, 27])

$$\theta_+ = \sqrt{-\frac{2}{N} \frac{\dot{b}}{b} \text{sign}(a)}, \quad (4.11)$$

$$\theta_- = -\sqrt{-\frac{2}{N} \frac{\dot{b}}{b}}. \quad (4.12)$$

The sign of a and \dot{b} determine if the region is trapped, anti-trapped or free. We can summarize the possibilities in Table 1. At this point, we now that regions outside the horizon ($a > 0$) are generically free regions. Similarly, regions inside the horizon ($a < 0$) are trapped or anti-trapped, as illustrated in Fig. 6. The sign of a is determined uniquely by the sign of v_2 , see (2.16b), and the latter is positive for all P_2 such that

$$f_2 < \frac{\lambda_2}{24K_1}. \quad (4.13)$$

However, which of both is the case, i.e. if the interior region is trapped or anti-trapped or if a transition happens as this depends on the position of the bounce relative to the horizons and thus the polymer functions and the Dirac observables K_1 and K_2 . To determine if the region between the horizon is trapped or anti-trapped, we have to look at f_1 . We recall that since $\dot{v}_1 = 2\dot{b}b^2 = 12\sqrt{n}v_1f_1\frac{f_2}{\lambda_2}$, and since $f_2 > 0$ we have $\text{sign}(\dot{b}) = \text{sign}(f_1)$.

So in this specific case, since $f_1' < 0$ between the horizons (cf Fig. 7), which means that $\dot{b} < 0$. So referring to Table 1, we deduce that the region between the horizons is anti-trapped. On the other hand, if we had chosen C such that the bounce lies within the horizons, the bounce surface would have been a transition surface between a trapped and an anti-trapped region. In this case, a proper black-to-white hole transition appears.

5 Large distance behaviour

We have seen that the polymerized black holes present many non-classical features, such as multiple horizons and bounces. However, we would still like these solutions to reproduce the standard Schwarzschild black hole at large distances. This was the motivation to restrict the polymer functions to satisfy (3.2). These restriction were based on experience with loop quantum cosmology and with the standard polymer black hole. In this section we derive these conditions showing that they are indeed necessary in order to recover the Schwarzschild solutions at large scales. However, it turns out that they are not sufficient. One needs a further condition, given by $f_2'' = 0$ which is satisfied by the sine polymerization, for instance.

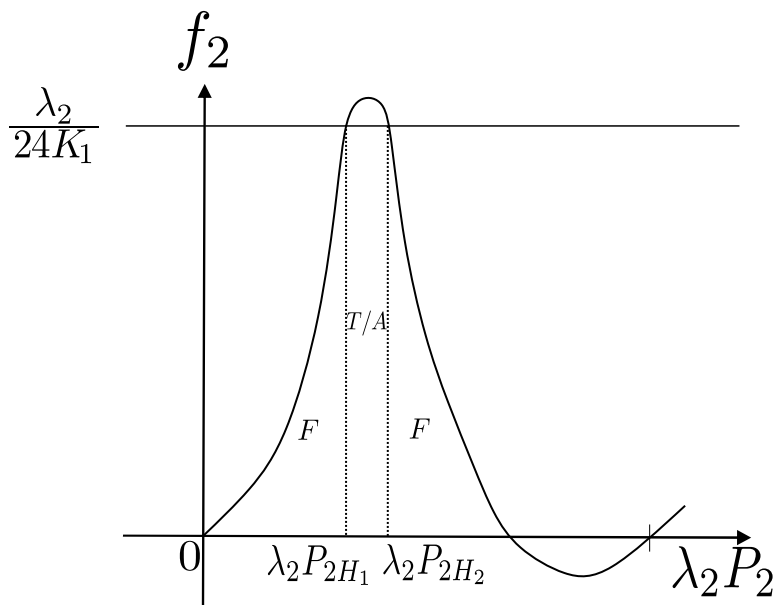


Figure 6: Plot of the polymerisation function f_2 chosen in Fig. 4. The horizontal line marks the threshold below which the region is free, and above which it is trapped/anti-trapped (T/A) depending on the sign of \dot{b} as shown in Table 1. The intersections correspond to two horizons. If f_1 is chosen so to have a single bounce, three situations can occur. Starting from the asymptotic region at $r \rightarrow +\infty$, namely, $\lambda_2 P_2 = 0$, the region between the horizon will be trapped (respectively anti-trapped) if the bounce occurs after the horizon (respectively before the horizon). If it occurs between the horizons, this region will be trapped and then anti-trapped.

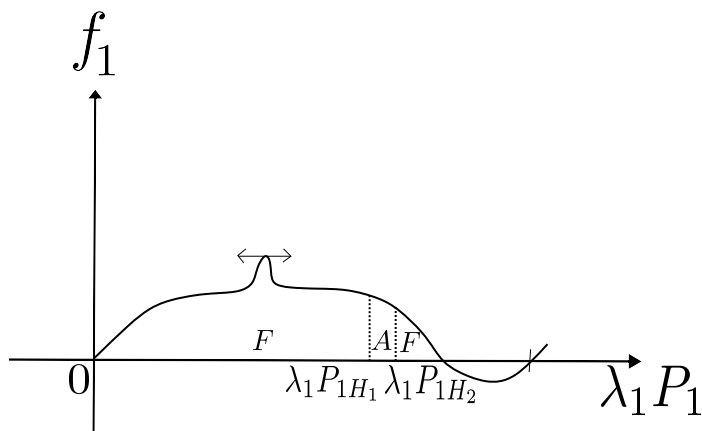


Figure 7: Plot of the polymerisation function f_1 chosen at the beginning of this section. The property free (F), trapped (T) or anti-trapped (A) of the spacetime is summarized on this plot.

Even though this condition was not explicitly required in the analysis of the previous Section, a quick inspection shows that it was not used anywhere, hence all the results there presented apply to the class of polymer functions correctly reproducing Schwarzschild metric's at large distances. The analysis presented in this Section is also somewhat heavier and requires additional notation, which is our reason to leave it for the end. It will also allow us to identify the mass of the black hole described by the generic solution (3.13).

An independent reason to study the large scale behaviour of the solutions concerns the interpretation of the spacetime *after* the bounce. If asymptotic flatness is recovered in that limit as well, it then becomes meaningful to talk about the mass of the white hole, and discuss the physics of the bouncing process in terms of asymptotic charges.

Let us now come to the technical aspects. The area radius is given by the variable b , hence the large scale limit is $b \rightarrow \infty$. However, while we can freely switch between r and P_2 as time variables, $b(\lambda_2 P_2)$ is not a monotonic function, recall analysis of Section 3.3 and Fig. 2.¹⁰ Therefore, we have to restrict our analysis to each branch of invertibility. Since we are interested in the asymptotic behaviour, we can focus on the two branches connected to the $r \rightarrow \pm\infty$ limits which corresponds to $b \rightarrow \pm\infty$. To study this, we will proceed with a perturbative expansion of the polymer functions with respect to $1/b$. Since the polymer functions depend implicitly on b via the solution $P_i(b)$, this will be a nested perturbative expansion that requires the use of the equations of motion.

5.1 Asymptotic behaviour

Let us consider the regions in P_i -space connected to the origin $P_i = 0$ (see Fig. 1). We denote P_i^\pm the two asymptotic fixed points reached in the limit $r \rightarrow \pm\infty$ respectively (we assume that in the $r \rightarrow \infty$ limit we flow to the semiclassical regime, hence $P_i^+ = 0$). We introduce the following notation,

$$x := \frac{1}{b}, \quad (5.1a)$$

$$z^\pm(x) := \lambda_1 P_1 - \lambda_1 P_1^\pm, \quad (5.1b)$$

$$y^\pm(x) := \lambda_2 P_2 - \lambda_2 P_2^\pm, \quad (5.1c)$$

so to have y^\pm and z^\pm vanish at the two fixed points of each trajectory. We denote the fixed points $x = 0^\pm$. To treat them at once with a single perturbative expansion we redefine the functions $f_i(\lambda_i P_i) \mapsto f_i(\lambda_i P_i - \lambda_i P_i^\pm)$, such that $f_i(0^\pm) = 0$. In the following, we will drop the superscript \pm from y and z to further lighten the notation.

In terms of these variables, the relevant components of (3.13) read

$$g_{\tau\tau}(x) = -x^2 \left(\frac{\lambda_2^2}{16f_2(y(x))^2} - \frac{3K_1\lambda_2}{2f_2(y(x))} \right), \quad (5.2a)$$

$$g_{xx}(x) = g_{bb}(x)/x^4. \quad (5.2b)$$

$$g_{bb}(x) = -\frac{\lambda_2^2 x^2}{16f_1'(z(x))^2 f_2(y(x))^2 g_{\tau\tau}(x)}, \quad (5.2c)$$

After some computations that can be found in Appendix B, one can show that these metric com-

¹⁰The origin of this is that $b(r)$ is no longer monotonic. This is why one can have b inverting behaviour going through a bounce while r runs smoothly over the whole real axis. Notice also that the value r_{bounce} can occur for either positive or negative values, depending on the polymer function and the parameters of the solution.

ponents at first order in x are

$$g_{\tau\tau} = -\frac{\lambda_2^2}{16f_2'(0^\pm)^2 y'(0^\pm)^2} \left(1 - \frac{2y'(0^\pm) (12K_1 f_2'(0^\pm)^2 + \lambda_2 f_2''(0^\pm))}{\lambda_2 f_2'(0^\pm)} x \right) + O(x^2), \quad (5.3a)$$

$$1/g_{bb} = f_1'(0^\pm)^2 \left(1 - \frac{24K_1 f_2'(0^\pm) y'(0^\pm)}{\lambda_2} x \right) + O(x^2). \quad (5.3b)$$

Since we have already fixed the area radius as coordinate, asymptotic flatness imposes

$$f_1'(0^\pm) = \pm 1. \quad (5.4)$$

Next, we still have the freedom of rescaling τ , which we use to reabsorb the prefactor in $g_{\tau\tau}$, so to have asymptotic flatness in the new time variable without restrictions on the polymer functions. On the other hand, area radius also requires that the time and radial components are the inverse of one another. Inspection of the above equations shows that this occurs if and only if

$$\frac{y'(0^\pm) f_2''(0^\pm)}{f_2'(0^\pm)} = 0 \quad \Rightarrow \quad f_2''(0^\pm) = 0 \quad (5.5)$$

by the previous conditions. In that case, the mass of the black hole is given by

$$M = \frac{12K_1 f_2'(0^\pm) y'(0^\pm)}{\lambda_2}. \quad (5.6)$$

Notice that it depends on K_2 via $y'(0^\pm)$, since K_2 appears in the relation between P_2 and b .¹¹

Consider now separately the two solutions for $r \rightarrow \pm\infty$. The corresponding values of M will generically be different, because $f_2'(0^\pm)$ and $y'(0^\pm)$ can take different values. Since $f_2'(0^\pm)$ and $y'(0^\pm)$ are both positive (respectively negative) in the black hole side (respectively in the white hole side), then the sign of the mass is only determined by the sign of K_1 , as in the unpolymerized case.

In summary, in order to obtain the Schwarzschild solution asymptotically at the fixed point, we need to impose the conditions (B.5), (5.4) and (5.5), i.e.

$$f_1'(0^\pm) = f_2'(0^\pm) \quad \text{and} \quad f_1'(0^\pm)^2 = 1 \quad \text{and} \quad f_2''(0^\pm) = 0. \quad (5.7)$$

This fixes three of the four derivatives of f_1 and f_2 up to the second order expansion. Note that in the case of the sine polymerisation, these conditions are automatically satisfied.

If we impose (5.7) at both fixed points, we obtain an evolution from an asymptotic Schwarzschild region to another asymptotic Schwarzschild region. Let us call the masses in the two regions M_{BH} and M_{WH} .¹² They are given by

$$M_{BH} = \frac{12K_1 f_2'(\lambda_2 P_2^-) y'(0^\pm)}{\lambda_2}, \quad M_{WH} = \frac{12K_1 f_2'(\lambda_2 P_2^+) y'(0^\pm)}{\lambda_2}. \quad (5.8)$$

¹¹One may ask how this mass enters the Kretschmann scalar, given schematically by (4.7). The complexity of that expression makes it however hard to answer this question, even for the simplest choices of polymer functions.

¹²These names have absolutely no meaning in terms of a black or white hole. Both asymptotic regions are Schwarzschild so both of these regions contain both, a black and a white hole. However, for the initial region, the black hole lies in the future and for the final region the white hole lies in the past. Depending on where the bounce is located w.r.t. the horizons (see the discussion in Sec. 4.4), an observer falling radially and freely starting in the initial region, will experience a black hole first, then see a transition from a trapped to an anti-trapped region, which the observer would call a white hole region until, she finds herself in an asymptotic exterior region of a Schwarzschild spacetime. This motivates the given notation, but there is no deeper physical meaning.

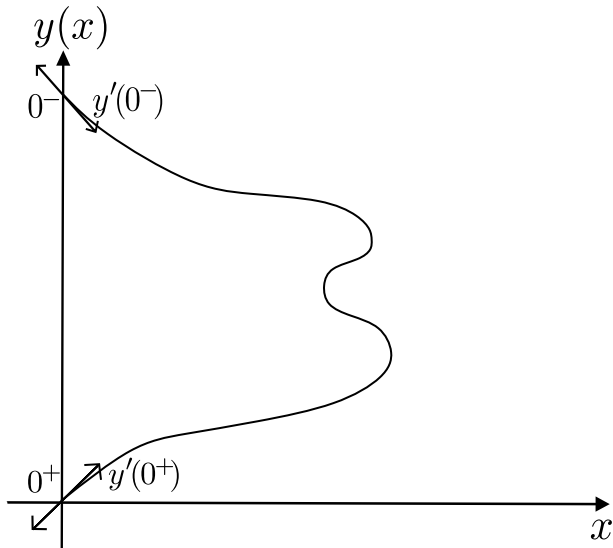


Figure 8: Sketch of the parametric solution $y(x)$. $y'_-(0^\pm)$ uniquely fixes the trajectory $y(x)$ and thus the final derivative $y'_+(0^\pm)$.

From (5.7) we see that $|f'_2(\lambda_2 P_2^-)| = |f'_2(\lambda_2 P_2^+)| = 1$. The evolution studied in Sec. 4.1 is such that no zeros of f_2 are crossed. Therefore, $f'_2(\lambda_2 P_2^-) = -f'_2(\lambda_2 P_2^+)$ and

$$\frac{M_{WH}}{M_{BH}} = -\frac{y'(0^\pm)}{y'(0^\pm)}. \quad (5.9)$$

Moreover, as it is illustrated in Figure 8, $y'(0^\pm)$ is positive in the black hole side and negative in the white hole side. This implies that the black hole mass and the white hole mass have the same sign. It is also possible to locally¹³ change coordinates in phase space from K_i to (M_{BH}, M_{WH}) .

Because the two asymptotic regions are disconnected, different asymptotic masses does not mean a violation of energy conservation: it only means that the time-like Killing vector cannot be normalized to one at both asymptotes. If one were interested in solutions with matching masses, one would be looking at a 1-dimensional subspace of the 2-dimensional phase space, determined by (5.9) once the polymer functions are chosen.

5.2 Taming quantum gravity effects outside the horizon

An obvious issue with non-singular black holes is to contain the deviations from general relativity not to spoil the macroscopic behaviour. To that end, we look at the next order term in the expansion (B.8a), and impose bounds on it. This requires $y^{(3)}(0^\pm)$, which can be computed as before from the equation of motion (B.3b) and taking the limit $x \rightarrow 0$. This leads to an recursive relation with

¹³The change of coordinates is given by (5.8) (recall that $y'(0^\pm)$ depends on K_2), and this may not be globally bijective. Consequently, we are limited to saying that this change of coordinates exists locally.

$y^{(3)}(0^\pm)$ on both sides, which can be solved to obtain

$$y^{(3)}(0^\pm) = \frac{y'(0^\pm)^3 f_2^{(3)}(0^\pm)}{2f_2'(0^\pm)}, \quad (5.10)$$

where we use explicitly the condition $f_2''(0^\pm) = 0$. We then find

$$g_{\tau\tau} = -\frac{\lambda_2^2}{16f_2'(0^\pm)^2 y'(0^\pm)^2} \left(1 - 2Mx - \text{sign}(f_2'(0^\pm)) \frac{y'(0^\pm)^2 f_2^{(3)}(0^\pm)}{2\lambda_2} x^2 \right) + O(x^3). \quad (5.11a)$$

The $O(x^2)$ term of $1/g_{bb}$ vanishes, as a consequence of $z''(0^\pm) = 0$ (cfr. (B.1)) and using the condition $f_2''(0^\pm) = 0$.

To keep the quantum corrections small outside of the horizon, we need the third term to be much smaller than the second for $b = x^{-1} \geq 2M$, namely

$$\frac{y'(0^\pm)^2 f_2^{(3)}(0^\pm)}{8\lambda_2 M^2} \ll 1. \quad (5.12)$$

This means that for given polymer functions, the condition is always satisfied for large enough black holes. Moreover, the expansion (5.11) allows us to obtain a criterion on the value of the area radius for which the deviations from the Schwarzschild metric become order one, given by

$$b \leq \sqrt{\left| \frac{y'(0)^2 f_2^{(3)}(0)}{2\lambda_2} \right|}. \quad (5.13)$$

A more precise characterization of the quantum corrections can be obtained studying the violations of the energy conditions, like for example in [49].

6 Conclusions

We have shown that it is possible to investigate generic features of effective models describing spherically symmetric black hole models inspired by loop quantum gravity taking into account the large freedom in choosing the polymerization functions. Most of the relevant global features of the solutions, as the location of horizons and the existence of bounces, are directly related to global features of the polymerization functions and the values of some Dirac observables or constants of motion. More precisely, the features of the polymerization function f_1 encode the physics of bounces, while f_2 and its relation to certain constants of motion determines the location of the Killing horizons. Consistency with the classical regime does not strongly restrict the infinite dimensional ambiguity in the polymerization procedure. However, it is worth pointing out that in addition to the usual requirements on $f_i(0^\pm)$ and $f_i'(0^\pm)$ that are derived from the naive continuum limit, our asymptotic analysis shows that in addition one needs to have $f_2''(0^\pm) = 0$. The number of bounces and the number of horizons can be freely specified by tuning the polymer functions and suitably choosing constants of motion. With respect to the list of properties of the BMM model (listed in Section 2.3) we conclude that all of them hold for an arbitrary polymerization except the shrinking of horizon. The deformation of the horizon can be freely controlled playing with the

choice of polymer function. We notice in passing that the model also allows for solutions with no horizons at all, where quantum effects produce violations of the classical Einstein's equations that can be seen as quantum stars made of 'matter' of an entirely quantum nature. The existence of such a large ambiguity in the construction of these models should not be surprising on general grounds [17, 18]. On the upper side this freedom could prove useful in the investigation of off-shell hypersurface deformation algebra [50–52]. Our analysis can also be applied to specific choices of non-sine polymer functions. It would be interesting to see whether it could be extended to different $\bar{\mu}$ -schemes like the one proposed in [19], and then be able to study analytically the behaviour of the geometry post-bounce [9].

Acknowledgements

The work of JM was made possible through the support of the ID# 61466 grant from the John Templeton Foundation, as part of the *The Quantum Information Structure of Spacetime* (QISS) Project (qiss.fr). The opinions expressed in this publication are those of the author(s) and do not necessarily reflect the views of the John Templeton Foundation.

A Boundary term

In this Appendix we recall the derivation of the minisuperspace Lagrangian (2.6). We consider a single boundary given by a r -constant hypersurfaces outside the horizon. The total action including the Gibbons-Hawking-York boundary term is

$$S[C] = \frac{1}{16\pi} \int dr \int_C d^3x \sqrt{-g} R - \frac{1}{8\pi} \int_C d^3x \sqrt{|h|} K. \quad (\text{A.1})$$

With the ansatz (2.1), we have

$$\sqrt{-g} R = \sin(\theta) \left(2\sqrt{\bar{n}} - \frac{4\bar{b}\dot{\bar{a}}\dot{\bar{b}}}{\sqrt{\bar{n}}} - \frac{2\bar{a}\dot{\bar{b}}^2}{\sqrt{\bar{n}}} + \frac{\bar{b}^2\dot{\bar{a}}\dot{\bar{n}}}{2\bar{n}^{3/2}} + \frac{2\bar{a}\bar{b}\dot{\bar{b}}\dot{\bar{n}}}{\bar{n}^{3/2}} - \frac{\bar{b}^2\ddot{\bar{a}}}{\sqrt{\bar{n}}} - \frac{4\bar{a}\bar{b}\ddot{\bar{b}}}{\sqrt{\bar{n}}} \right), \quad (\text{A.2})$$

hence the Einstein-Hilbert term gives

$$\frac{1}{16\pi} \int_C d^3x \sqrt{-g} R = \frac{\ell_0 \sqrt{\bar{n}}}{2} \left(\frac{\dot{\bar{a}}\dot{\bar{b}}\dot{\bar{b}}}{\bar{n}} + \frac{\bar{a}\dot{\bar{b}}^2}{\bar{n}} + 1 \right) - \ell_0 \frac{d}{dr} \left(\frac{\dot{\bar{a}}\dot{\bar{b}}^2}{4\sqrt{\bar{n}}} + \frac{\bar{a}\bar{b}\dot{\bar{b}}}{\sqrt{\bar{n}}} \right). \quad (\text{A.3})$$

Coming to the boundary term, the unit-normal to the r foliation is, outside the horizon,

$$n = \sqrt{\frac{\bar{n}(r)}{\bar{a}(r)}} dr, \quad n^2 = 1. \quad (\text{A.4})$$

To this we associate the induced metric and extrinsic curvature

$$q_{\mu\nu} = g_{\mu\nu} - n_a n_b, \quad K_{\mu\nu} = q_{\mu}^{\rho} \nabla_{\rho} n_{\nu} = \frac{1}{2} \mathcal{L}_n q_{\mu\nu}. \quad (\text{A.5})$$

With the ansatz (2.1), we find

$$q = -\bar{a}\bar{b}^4 \sin(\theta)^2, \quad K = \frac{\dot{\bar{a}}}{2\sqrt{\bar{n}\bar{a}}} + \frac{2\sqrt{\bar{a}}\dot{\bar{b}}}{\sqrt{\bar{n}\bar{b}}}. \quad (\text{A.6})$$

Hence the boundary term gives

$$\frac{1}{8\pi} \int d^3x \sqrt{h} K = \ell_0 \left(\frac{\dot{\bar{a}}\bar{b}^2}{4\sqrt{\bar{n}}} + \frac{\bar{a}\dot{\bar{b}}}{\sqrt{\bar{n}}} \right). \quad (\text{A.7})$$

Adding up, we recover (2.6).

B Asymptotic expansion of the metric components

In this Appendix, we provide details on the asymptotic expansion of the metric components (5.2) leading to (5.3). First, one can note that the only functions whose expansions are needed are $f_2(y(x))$ and $f_1'(z(x)) = \frac{df_1}{dz}(z(x))$, while all dependencies of $f_1(z(x))$ have been replaced by the use of the Dirac observable K_1 and Eq. (3.8). This also fixed the function

$$z(x) = f_1^{-1} (3\lambda_1 K_1 x^3 / 2). \quad (\text{B.1})$$

With these notations, the formal Taylor expansions are given by

$$f_2(y(x)) = f_2'(0^\pm) y'(0^\pm) x + \frac{1}{2} (f_2''(0^\pm) y'(0^\pm)^2 + f_2'(0^\pm) y''(0^\pm)) x^2 + O(x^3), \quad (\text{B.2a})$$

$$f_1'(z(x)) = f_1'(0^\pm) + f_1''(0^\pm) z'(0^\pm) x + \frac{1}{2} (f_1^{(3)}(0^\pm) z'(0^\pm)^2 + f_1''(0^\pm) z''(0^\pm)) x^2 + O(x^3) \quad (\text{B.2b})$$

$$\stackrel{(\text{B.1})}{=} f_1'(0^\pm) + O(x^3), \quad (\text{B.2c})$$

with $f_i^{(n)}$ denoting the n -th derivative w.r.t. y or z , respectively, while $y' = dy/dx$ and respectively, y'' , z' and z'' . It was assumed and will be in the following that $f_i'(0^\pm) \neq 0$, which would also violate the classical limit. These expressions are formal however, as the derivatives $y'(0^\pm)$, $y''(0^\pm)$ are not specified. The derivatives z' and z'' follow from (B.1) and we see that linear and quadratic order vanish exactly. From the equations of motion (3.4) follow the expressions

$$y'(x) = \frac{f_2(y(x))}{x f_1'(z(x))}, \quad (\text{B.3a})$$

$$y''(x) = \frac{f_2'(y(x)) f_2(y(x))}{x^2 f_1'(z(x))^2} - \frac{f_2(y(x))}{x^2 f_1'(z(x))} - \frac{9K_1 \lambda_1 f_1''(z(x)) f_2(y(x)) x}{2 f_1'(z(x))^3}, \quad (\text{B.3b})$$

Extracting $y'(0^\pm)$ requires then

$$y'(0^\pm) = \lim_{x \rightarrow 0} y'(x) = \frac{f_2'(0^\pm)}{f_1'(0^\pm)} y'(0^\pm). \quad (\text{B.4})$$

This implies

$$f_1'(0^\pm) = f_2'(0^\pm), \quad (\text{B.5})$$

with $y'(0^\pm)$ unconstrained.¹⁴ Similarly, for the second derivative, we get

$$y''(0^\pm) = \lim_{x \rightarrow 0} y''(x) = \frac{y'(0^\pm)^2 f_2''(0^\pm) + f_2'(0^\pm) y''(0^\pm)}{2 f_1'(0^\pm)}, \quad (\text{B.6})$$

¹⁴Recall that the fixed points are not part of the phase space but only reached asymptotically. This eliminates the possibility of solving (B.4) taking $y'(0^\pm) \equiv 0$.

which can be solved to obtain

$$y''(0^\pm) = \frac{y'(0^\pm)^2 f_2''(0^\pm)}{f_2'(0^\pm)}. \quad (\text{B.7})$$

Here we again used the constraint $f_1'(0^\pm) = f_2'(0^\pm)$. This makes the expansions (B.2) explicit and allows to compute the metric functions, leading to

$$g_{\tau\tau} = -\frac{\lambda_2^2}{16 f_2'(0^\pm)^2 y'(0^\pm)^2} \left(1 - \frac{2y'(0^\pm) (12K_1 f_2'(0^\pm)^2 + \lambda_2 f_2''(0^\pm))}{\lambda_2 f_2'(0^\pm)} x \right) + O(x^2), \quad (\text{B.8a})$$

$$1/g_{bb} = f_1'(0^\pm)^2 \left(1 - \frac{24K_1 f_2'(0^\pm) y'(0^\pm)}{\lambda_2} x \right) + O(x^2). \quad (\text{B.8b})$$

References

- [1] C. G. Callan, Jr., S. B. Giddings, J. A. Harvey and A. Strominger, *Evanescent black holes*, Phys. Rev. D **45** (1992), no. 4 R1005 [[hep-th/9111056](#)].
- [2] A. Ashtekar, F. Pretorius and F. M. Ramazanoglu, *Surprises in the Evaporation of 2-Dimensional Black Holes*, Phys. Rev. Lett. **106** (2011) 161303 [[1011.6442](#)].
- [3] A. Ashtekar, T. Pawłowski and P. Singh, *Quantum Nature of the Big Bang: Improved dynamics*, Phys. Rev. D **74** (2006) 084003 [[gr-qc/0607039](#)].
- [4] A. Ashtekar and P. Singh, *Loop quantum cosmology: a status report*, Classical and Quantum Gravity **28** (nov, 2011) 213001 [[arXiv:1108.0893](#) [[gr-qc](#)]].
- [5] J. G. Kelly, R. Santacruz and E. Wilson-Ewing, *Effective loop quantum gravity framework for vacuum spherically symmetric spacetimes*, Phys. Rev. D **102** (2020), no. 10 106024 [[2006.09302](#)].
- [6] J. B. Achour, F. Lamy, H. Liu and K. Noui, *Non-singular black holes and the Limiting Curvature Mechanism: A Hamiltonian perspective*, J. Cosmol. Astropart. Phys. **2018** (2017), no. 05 72 [[1712.03876](#)].
- [7] A. Ashtekar, J. Olmedo and P. Singh, *Quantum Transfiguration of Kruskal Black Holes*, Physical Review Letters **121** (dec, 2018) 241301 [[arXiv:1806.00648](#) [[gr-qc](#)]].
- [8] N. Bodendorfer, F. M. Mele and J. Münch, *Effective quantum extended spacetime of polymer Schwarzschild black hole*, Classical and Quantum Gravity **36** (oct, 2019) 195015 [[arXiv:1902.04542](#) [[gr-qc](#)]].
- [9] E. Alesci, S. Bahrami and D. Pranzetti, *Asymptotically de Sitter universe inside a Schwarzschild black hole*, Physical Review D **102** (sep, 2020) 066010 [[arXiv:2007.06664](#) [[gr-qc](#)]].
- [10] L. Modesto, *Loop quantum black hole*, Class. Quant. Grav. **23** (2006) 5587–5602 [[gr-qc/0509078](#)].
- [11] A. Ashtekar and M. Bojowald, *Quantum geometry and the Schwarzschild singularity*, Class. Quant. Grav. **23** (2006) 391–411 [[gr-qc/0509075](#)].
- [12] V. Taveras, *Corrections to the Friedmann equations from loop quantum gravity for a universe with a free scalar field*, Physical Review D **78** (sep, 2008) 064072 [[arXiv:0807.3325](#) [[gr-qc](#)]].
- [13] M. Bojowald, *Comment on “Towards a quantum notion of covariance in spherically symmetric loop quantum gravity”*, Phys. Rev. D **105** (2022), no. 10 108901 [[2203.06049](#)].
- [14] M. Bojowald, *Noncovariance of “covariant polymerization” in models of loop quantum gravity*, Phys. Rev. D **103** (2021), no. 12 126025 [[2102.11130](#)].
- [15] M. Bojowald, *No-go result for covariance in models of loop quantum gravity*, Phys. Rev. D **102** (2020), no. 4 046006 [[2007.16066](#)].

- [16] M. Bojowald, *Comment (2) on "Quantum Transfiguration of Kruskal Black Holes"*, [1906.04650](#).
- [17] L. Amadei, A. Perez and S. Ribisi, *The landscape of polymer quantum cosmology*, [2203.07044](#).
- [18] A. Perez, *On the regularization ambiguities in loop quantum gravity*, Phys. Rev. D **73** (2006) 044007 [[gr-qc/0509118](#)].
- [19] E. Alesci, S. Bahrami and D. Pranzetti, *Quantum gravity predictions polymer BHv2 for black hole interior geometry*, Phys. Lett. B **797** (2019) 134908 [[1904.12412](#)].
- [20] M. Varadarajan, *Euclidean LQG Dynamics: An Electric Shift in Perspective*, Class. Quant. Grav. **38** (2021), no. 13 135020 [[2101.03115](#)].
- [21] M. Varadarajan and A. Perez, *public and private discussion during LOOPs 22 conference*, July 2022.
- [22] B. Vakili, *Classical Polymerization of the Schwarzschild Metric*, Advances in High Energy Physics **2018** (sep, 2018) 1–10 [[arXiv:1806.01837](#) [[hep-th](#)]].
- [23] A. Corichi and P. Singh, *Loop quantization of the Schwarzschild interior revisited*, Classical and Quantum Gravity **33** (mar, 2016) 055006 [[arXiv:1506.08015](#) [[gr-qc](#)]].
- [24] L. Modesto, *Semiclassical Loop Quantum Black Hole*, International Journal of Theoretical Physics **49** (aug, 2010) 1649–1683 [[arXiv:0811.2196](#) [[gr-qc](#)]].
- [25] C. G. Böhrmer and K. Vandersloot, *Loop quantum dynamics of the Schwarzschild interior*, Physical Review D **76** (nov, 2007) 104030 [[arXiv:0709.2129](#) [[gr-qc](#)]].
- [26] J. Ben Achour, F. Lamy, H. Liu and K. Noui, *Polymer Schwarzschild black hole: An effective metric*, EPL (Europhysics Letters) **123** (aug, 2018) 20006 [[arXiv:1803.01152](#) [[gr-qc](#)]].
- [27] A. Ashtekar, J. Olmedo and P. Singh, *Quantum extension of the Kruskal spacetime*, Physical Review D **98** (dec, 2018) 126003 [[arXiv:1806.02406](#) [[gr-qc](#)]].
- [28] N. Bodendorfer, F. M. Mele and J. Münch, *A note on the Hamiltonian as a polymerisation parameter*, Classical and Quantum Gravity **36** (sep, 2019) 187001 [[arXiv:1902.04032](#) [[gr-qc](#)]].
- [29] N. Bodendorfer, F. M. Mele and J. Münch, *Mass and horizon Dirac observables in effective models of quantum black-to-white hole transition*, Classical and Quantum Gravity **38** (may, 2021) 095002 [[arXiv:1912.00774](#) [[gr-qc](#)]].
- [30] N. Bodendorfer, F. M. Mele and J. Münch, *(b,v)-type variables for black to white hole transitions in effective loop quantum gravity*, Physics Letters B **819** (aug, 2021) 136390 [[arXiv:1911.12646](#) [[gr-qc](#)]].
- [31] M. Assanioussi, A. Dapor and K. Liegener, *Perspectives on the dynamics in a loop quantum gravity effective description of black hole interiors*, Physical Review D **101** (jan, 2020) 026002 [[arXiv:1908.05756](#) [[gr-qc](#)]].
- [32] J. G. Kelly, R. Santacruz and E. Wilson-Ewing, *Effective loop quantum gravity framework for vacuum spherically symmetric spacetimes*, Physical Review D **102** (nov, 2020) 106024 [[arXiv:2006.09302](#) [[gr-qc](#)]].
- [33] J. G. Kelly, R. Santacruz and E. Wilson-Ewing, *Black hole collapse and bounce in effective loop quantum gravity*, Classical and Quantum Gravity **38** (feb, 2021) 04LT01 [[arXiv:2006.09325](#) [[gr-qc](#)]].
- [34] R. Gambini, J. Olmedo and J. Pullin, *Spherically symmetric loop quantum gravity: analysis of improved dynamics*, Classical and Quantum Gravity **37** (oct, 2020) 205012 [[arXiv:2006.01513](#) [[gr-qc](#)]].
- [35] M. Geiller, E. R. Livine and F. Sartini, *Symmetries of the black hole interior and singularity regularization*, SciPost Physics **10** (jan, 2021) 022 [[arXiv:2010.07059](#) [[gr-qc](#)]].
- [36] F. Sartini and M. Geiller, *Quantum dynamics of the black hole interior in loop quantum cosmology*, Physical Review D **103** (mar, 2021) 066014 [[arXiv:2010.07056](#) [[gr-qc](#)]].
- [37] M. Bouhmadi-López, S. Brahma, C.-Y. Chen, P. Chen and D.-h. Yeom, *Asymptotic non-flatness of an*

- effective black hole model based on loop quantum gravity*, Physics of the Dark Universe **30** (dec, 2020) 100701 [[arXiv:1902.07874](#) [\[gr-qc\]](#)].
- [38] W.-C. Gan, N. O. Santos, F.-W. Shu and A. Wang, *Properties of the spherically symmetric polymer black holes*, Physical Review D **102** (dec, 2020) 124030 [[arXiv:2008.09664](#) [\[gr-qc\]](#)].
- [39] A. García-Quismondo and G. A. Mena Marugán, *Exploring Alternatives to the Hamiltonian Calculation of the Ashtekar-Olmedo-Singh Black Hole Solution*, Frontiers in Astronomy and Space Sciences **8** (jul, 2021) 115 [[arXiv:2107.00947](#) [\[gr-qc\]](#)].
- [40] R. Gambini, J. Olmedo and J. Pullin, *Loop Quantum Black Hole Extensions Within the Improved Dynamics*, Frontiers in Astronomy and Space Sciences **8** (jun, 2021) 74 [[arXiv:2012.14212](#) [\[gr-qc\]](#)].
- [41] B. Elizaga Navascués, A. García-Quismondo and G. A. Mena Marugán, *Hamiltonian formulation and loop quantization of a recent extension of the Kruskal spacetime*, Phys. Rev. D **106** (2022), no. 4 043531 [[2208.00425](#)].
- [42] M. Geiller, E. R. Livine and F. Sartini, *Dynamical symmetries of homogeneous minisuperspace models*, Phys. Rev. D **106** (2022), no. 6 064013 [[2205.02615](#)].
- [43] C. Rovelli and E. Wilson-Ewing, *Why are the effective equations of loop quantum cosmology so accurate?*, Phys. Rev. D **90** (2014), no. 2 023538 [[1310.8654](#)].
- [44] S. A. Hayward, *Formation and evaporation of regular black holes*, Phys. Rev. Lett. **96** (2006) 031103 [[gr-qc/0506126](#)].
- [45] C. Rovelli and F. Vidotto, *Planck stars*, Int. J. Mod. Phys. D **23** (2014), no. 12 1442026 [[1401.6562](#)].
- [46] M. Bojowald, *No-go result for covariance in models of loop quantum gravity*, Physical Review D **102** (aug, 2020) 046006 [[arXiv:2007.16066](#) [\[gr-qc\]](#)].
- [47] H. M. Haggard and C. Rovelli, *Quantum-gravity effects outside the horizon spark black to white hole tunneling*, Phys. Rev. D **92** (2015), no. 10 104020 [[1407.0989](#)].
- [48] A. Rignon-Bret and C. Rovelli, *Black to white transition of a charged black hole*, Phys. Rev. D **105** (2022), no. 8 086003 [[2108.12823](#)].
- [49] T. De Lorenzo, C. Pacilio, C. Rovelli and S. Speziale, *On the Effective Metric of a Planck Star*, Gen. Rel. Grav. **47** (2015), no. 4 41 [[1412.6015](#)].
- [50] M. Bojowald, S. Brahma, U. Buyukcam and F. D'Ambrosio, *Hypersurface-deformation algebroids and effective spacetime models*, Phys. Rev. D **94** (2016), no. 10 104032 [[1610.08355](#)].
- [51] C. Blohmann, M. Schiavina and A. Weinstein, *A Lie-Rinehart algebra in general relativity*, [2201.02883](#).
- [52] A. Alonso-Bardaji and D. Brizuela, *Anomaly-free deformations of spherical general relativity coupled to matter*, Physical Review D **104** (oct, 2021) 084064 [[arXiv:2106.07595](#) [\[gr-qc\]](#)].